A LOW-POWER, REAL-TIME, S-BAND RADAR IMAGING SYSTEM

Gregory L. Charvat, Leo C. Kempel, and Edward J. Rothwell
Dept. of Electrical and Computer Engineering, 2120 Engineering Building,
Michigan State University, East Lansing, MI 48824

Chris Coleman
Integrity Applications Incorporated
5180 Parkstone Drive
Suite 260, Chantilly, VA 20151

ABSTRACT

A real-time S-band radar imaging system will be shown in this paper that uses a spatially diverse antenna array connected to a highly sensitive linear FM radar system and uses a synthetic aperture radar (SAR) imaging algorithm to produce real-time radar imagery. The core of this radar system is a high-sensitivity, range gated, radar architecture. Previous work has demonstrated the effectiveness of this radar architecture for applications requiring low-power and high sensitivity for imaging through lossy dielectric slabs at S-band and in free space at both S and X bands. From these results it was decided to develop a real-time S-band SAR imaging system. This is achieved by constructing a spatially diverse antenna array that plugs directly into a pair of S-band transmit and receive radar front ends; thereby providing the ability for real-time SAR imaging of objects. The radar system chirps from approximately 2 GHz to 4 GHz at various rates from 700 microseconds to 10 milliseconds. Transmit power is adjustable from approximately 1 milliwatt or less. The image update rate is approximately one image every 1.9 seconds when operating at a chirp rate of 2.5 milliseconds. This system is capable of producing imagery of target scenes made up of objects as small as 1.25 inch tall nails in free space without the use of coherent integration. Previous applications for this radar system include imaging through dielectric slabs. It will be shown in this paper that this radar system could also be useful for real-time radar imaging of low RCS targets at S-band.

Keywords: RCS Measurements, Real-Time RCS Measurements, S-band Measurements, S-band Radar, Synthetic Aperture Radar, Real-Time Synthetic Aperture Radar, FMCW, Linear FM

1.0 Introduction

A real-time S-band SAR imaging system was recently developed by the Michigan State University Electromagnetics Research Group for the purpose of through-slab radar imaging. This radar system is a switched antenna array, where bi-static combinations of antennas are routed to the transmitter and receiver through electronic switches allowing for the radar phase center to be moved rapidly down a known path along the array. Range profiles acquired along this path are fed into a SAR imaging algorithm which produces a radar image of the target scene. This process is repeated in a loop producing real-time imagery of the target scene.

Previous switched antenna arrays used for through-slab radar imaging include [1] through [9]. Other switched antenna arrays used for free-space radar imaging include [10] through [12]. The system shown in this paper is a large (compared to a wavelength) S-band array. The radar unit that plugs into this array is a highly sensitive linear FM architecture developed for the purpose of through-slab imaging [14]. It will be shown in this paper that this radar system could also be used for purpose of real-time SAR imaging of low RCS targets at short ranges, where it will be shown to be capable of imaging free-space target scenes made up of targets as small as 1.25 inch tall nails.

Section 2.0 will discuss the high sensitivity linear FMCW radar architecture. Section 3.0 will provide technical details of the system implementation. Section 4.0 will show free-space imaging results of low RCS targets. Section 5.0 will summarize the results and discuss future work.

2.0 Radar Architecture

The resulting range to target information from a de-correlated linear FM radar chirp is in the form of low frequency beat tones. This was shown for the case of FMCW radar in [15] through [19]. The more distant the target the higher frequency the de-correlated beat tone. For this reason it is possible to implement a short duration range gate in a linear FM radar system by simply placing a band pass filter (BPF) on the output of the video amplifier in a traditional design FMCW radar system. However, this is challenging to implement in practice because it is difficult to design effective high Q band pass filters at base-band with comparable performance to communications IF filters. Much higher performance

BPF's are available in the form of widely used IF communications filters which operate at high frequencies. These filters are found in two-way radios, various types of communication, and television receivers. Examples of these IF filters include; crystal filters, ceramic filters, SAW filters, and mechanical filters.

These communications IF filters typically operate at standard IF frequencies of 10.7 MHz, 21.4 MHz, 455 KHz, 49 MHz and etc. These filters are high Q, where Q is defined as [20]

$$Q = \frac{f_c}{B},$$

where f_c = center frequency of the BPF and $B = -3$ dB bandwidth of the filter. A typical operating frequency of a crystal filter would be $f_c = 10.7$ MHz with a bandwidth of $B = 7.5$ KHz. The resulting Q of this filter would be $Q = 1426.7$. High Q's such as this are difficult to achieve with BPF designs at base-band audio frequencies.

The radar architecture shown in this paper uses high Q IF filters to create a short duration range gate, while at the same time, reducing receiver noise bandwidth B_n causing a dramatic increase in receiver sensitivity. With this design; the shorter duration the range gate, the more sensitive the radar receiver.

A simplified block diagram of the radar system is shown in Figure 1. In the following explanation amplitude coefficients will be ignored. OSC1 is a high frequency tunable oscillator. The frequency output of OSC1 is f_{BFO} which can be represented by the equation:

$$BFO(t) = \cos(2\pi f_{BFO} t).$$

The output of OSC1 is fed into the IF port of MXR1. The LO port of MXR1 is driven by OSC2. OSC2 is a 2 GHz to 4 GHz voltage tuned YIG oscillator. OSC2 is linear FM modulated by a ramp input where the output of OSC2 can be represented by the equation:

$$LO(t) = \cos\left(2\pi(2\cdot 10^9 + c_r t)t\right)$$

where c_r is the chirp rate in Hz/seconds.

OSC1 and OSC2 are mixed together in MXR1 to produce the transmit signal which is then amplified by power amplifier PA1. The output of PA1 is fed into the transmit antenna ANT1 and propagated out towards the target scene. The transmitted signal out of ANT1is $TX(t)$, where:

$$TX(t) = LO(t)\cdot BFO(t).$$

After some simplification this becomes

$$TX(t) = \cos\left(2\pi(2\cdot 10^9 + c_r t)t + 2\pi f_{BFO} t\right) + \cos\left(2\pi(2\cdot 10^9 + c_r t)t - 2\pi f_{BFO} t\right).$$

The transmitted waveform $TX(t)$ is radiated out to the target scene, reflected off of a target, delayed by some round trip time t_{delay} and propagated back to the receiver antenna ANT2. The received signal at ANT2 is represented by the equation:

$$RX(t) = \cos\left(2\pi(2\cdot 10^9 + c_r t)(t - t_{delay}) + 2\pi f_{BFO}(t - t_{delay})\right) + \cos\left(2\pi(2\cdot 10^9 + c_r t)(t - t_{delay}) - 2\pi f_{BFO}(t - t_{delay})\right).$$

The output of ANT2 is amplified by LNA1 and fed into MXR2. The LO port of MXR2 is fed by OSC2. The IF output of MXR2 is the product

$$IF(t) = LO(t)\cdot RX(t).$$

As a practical consideration the IF port of MXR2 can not output microwave frequencies so the high frequency terms can be dropped. So the resulting multiplication of the above equation results in:

$$IF(t) = \cos\left[-2\pi(2\cdot 10^9 + c_r t)t_{delay} + 2\pi f_{BFO}(t - t_{delay})\right] + \cos\left[-2\pi(2\cdot 10^9 + c_r t)t_{delay} - 2\pi f_{BFO}(t - t_{delay})\right].$$

As another practical consideration the DC blocking capacitors in the IF amplifier AMP1 will reject the DC phase terms, resulting in:

$$IF(t) = \cos\left(2\pi(f_{BFO} - c_r t_{delay})t\right) + \cos\left(2\pi(f_{BFO} + c_r t_{delay})t\right).$$

$IF(t)$ is fed into the high Q IF filter FL1. FL1 has a center frequency of f_c and a bandwidth of BW. OSC1

is set to a frequency such that $f_{BFO} \geq \frac{BW}{2} + f_c$ causing FL1 to pass only the lower sideband of $IF(t)$, thus causing the output of FL1 to be:

$$FIL(t) = \begin{cases} \cos\left(2\pi(f_{BFO} - c_r t_{delay})t\right) & if \quad \frac{-BW}{2} + f_c < f_{BFO} - c_r t_{dealy} < \frac{BW}{2} + f_c \\ 0 & otherwise \end{cases} \tag{1}$$

Only beat frequencies in the range of

$$\frac{-BW}{2} + f_c < f_{BFO} - c_r t_{delay} < \frac{BW}{2} + f_c$$

are passed through IF filter FL1. Since in an FMCW radar system the range to target is directly proportional to the beat frequency $c_r t_{delay}$, then the band limited IF signal (which is proportional to downrange target location) is effectively a hardware range-gate.

Increasing the bandwidth of FL1 increases the range-gate duration. Decreasing the bandwidth of FL1 decreases the range-gate duration. It is for this reason that the range-gate is adjustable if a number of different bandwidth filters were used, switched in and out of the IF signal chain.

If f_{BFO} were increased then the filter FL1 passes only signals that fit the equality in Equation 1. Since the $c_r t$ term is subtracted from f_{BFO} then the $c_r t$ term would have to be greater in size to compensate for a higher f_{BFO} frequency in order to let the IF signals pass through FL1. Thus, the filter FL1 would only pass beat tones further down range but at the same range duration in length if the frequency f_{BFO} were increased. So the range-gate is adjustable in physical downrange location (physical down range time delay).

In addition to these desirable properties the narrow bandwidth of FL1 greatly increases the receiver sensitivity because FL1 decreases the noise bandwidth presented to the radar digitizer. It is well known in communication receiver theory that the more narrow the IF bandwidth the better the sensitivity. According to [21] for an ideal receiver the sensitivity of a SSB or CW receiver can be approximated by calculating the minimum detectable signal (MDS) which is related directly to the IF bandwidth:

$$MDS_{dBm} = -174 + 10\log_{10} B_n + NF, \tag{2}$$

where:

B_n = noise bandwidth of the receiver (Hz), which is the IF bandwidth for an ideal receiver:

-174 dBm is the available thermal noise power per Hz at room temperature of $290^\circ K$:

$NF = 3.3$dB front end noise figure for the Mini-Circuits broad-band amplifier that is used in the radar system developed in this paper.

In the case of the radar system developed for this research, FL1 has an $f_c = 10.7$ MHz and $BW = 7.5$KHz. According to Equation 2 the receiver sensitivity would be -131.9 dB without signal processing gain. In addition to high sensitivity the bandwidth would provide a short duration range-gate of 9.375 nS for a chirp rate of $c_r = 800$ GHz/second. This sensitivity performance is significantly greater than a short pulsed radar system with a 9.375 nS range-gate, requiring an IF bandwidth of approximately 100 MHz to capture a single pulse, which according to Equation 2 would provide a sensitivity of approximately -90.4 dBm. Additional gain for both types of systems, short pulse and high sensitivity linear FM, can be achieved through signal processing coherent integration and other methods.

One last step occurs in the signal chain shown in Figure 1 where the output of FL1 is downconverted to base band through MXR3. The LO port of MXR3 is driven by OSC1 and the output of MXR3 is fed through Video Amp1 which can be represented by the equation:

$$Video(t) = BFO(t) \cdot FIL(t).$$

Video Amp1 is an active low pass filter, rejecting the higher frequency component of the cosine multiplication, resulting in the video output signal:

$$Video(t) = \begin{cases} \cos(2\pi c_r t_{delay} t) & if \quad \frac{-BW}{2} + f_c - f_{BFO} < c_r t_{delay} < \frac{BW}{2} + f_c - f_{BFO} \\ 0 & otherwise \end{cases}.$$

The result is a range gated base-band video signal similar to the radar systems shown in [15] through [19]. This result is identical to a traditional FMCW systems except that this signal is band limited by a high Q bandpass filter with an adjustable center frequency which effectively range-gates the video signal that is fed into the digitizer. This architecture will be used to implement the radar imaging system shown in the next section.

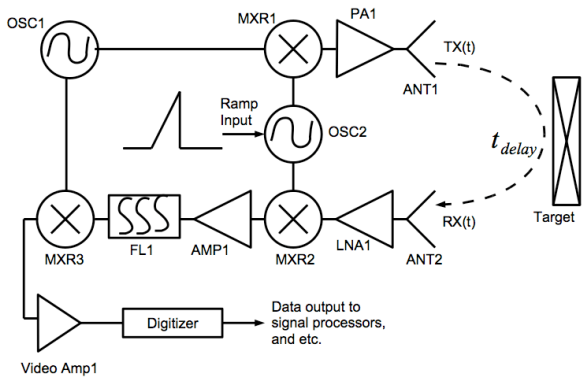

Figure 1 - Simplified block diagram of the high sensitivity range-gated FMCW radar system.

3. System Implementation

The hardware implementation of this radar system is a switched antenna array where the transmitter is connected to a transmit sub-array. The receiver is connected to a receive sub-array. A fan-out solid state microwave switch matrix connects the transmitter to one transmit element at a time as shown in Figure 2. Another fan-out solid state microwave switch matrix connects the receiver to one receive element at a time as shown in Figure 3. Combinations of transmit and receive elements cause the phase center of the resulting bi-static pair to move laterally in space. A drawing of the element locations for both the transmit and receive sub-arrays and their resulting phase centers is shown in Figure 4. This array results in one phase center every 2 inches across the length of the array.

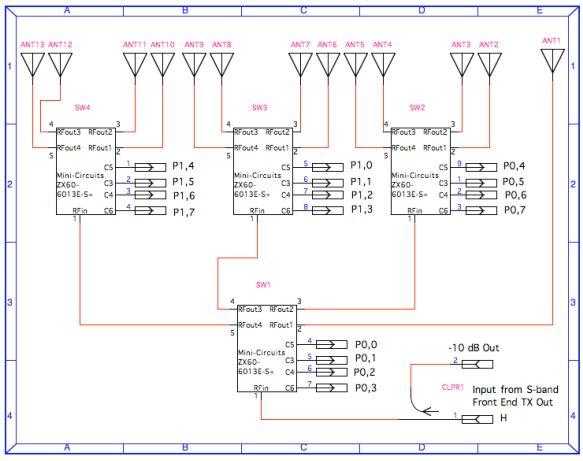

Figure 2 – Block diagram of the transmit sub-array.

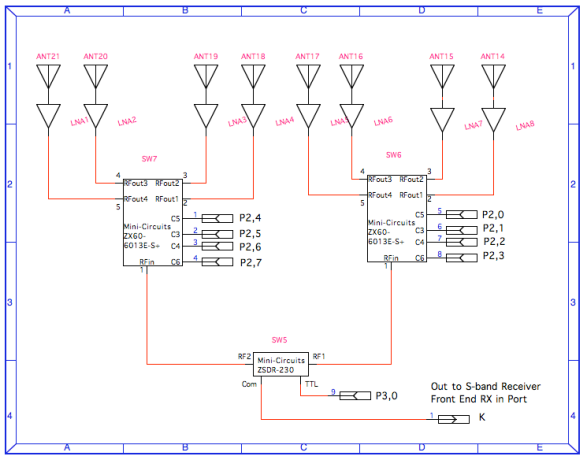

Figure 3 – Block diagram of the receive sub-array.

A picture of the radar system is shown in Figure 5. The radar is chirped from approximately 2 GHz to 4 GHz resulting in 2 GHz of chirp bandwidth. The chirp time is 2.5 milli-seconds. The IF filter center frequency is 10.7 MHz with a bandwidth of 7.5 KHz. The IF bandwidth is set by two ECS-10.7-7.5B crystal filters in series with a number of IF amplifiers and adjustable attenuators in between so as to maximize the usable dynamic range of the digitizer. The radar video output is digitized by a 16 bit 200 KSPS ADC. Receiver sensitivity was measured to be < -125 dBm. The system dynamic range was measured to be > 120 dB. The transmit power is approximately 1 milli-watt at the antenna terminals. All of the transmit and receive antennas are linearly tapered slot antennas (see [22] through [28]) cut from FR-4. The antenna polarization is vertical. The array consists of 13 transmit antennas and 8 receive antennas. The receive antennas have LNA's mounted on them. The aperture spacing across the linear rail is 2 inches spanning 86 inches in length. Complete design details of this system are presented in [14].

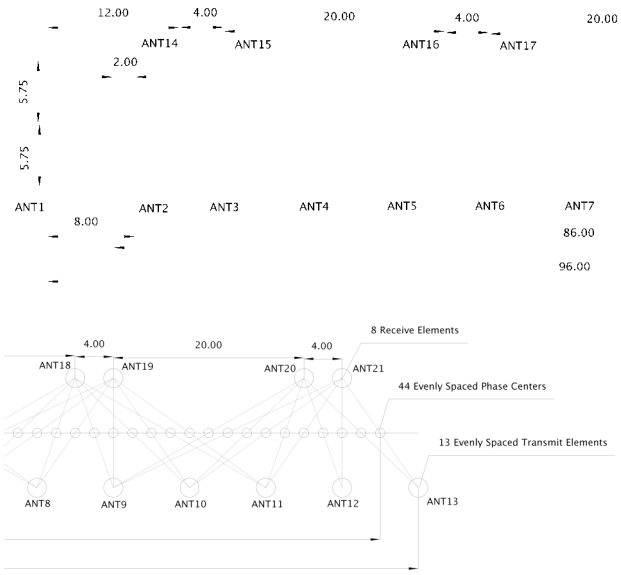

Figure 4 - Physical layout (all units are in inches), of the array with phase center positions shown.

Figure 5 – The real-time S-band radar imaging system.

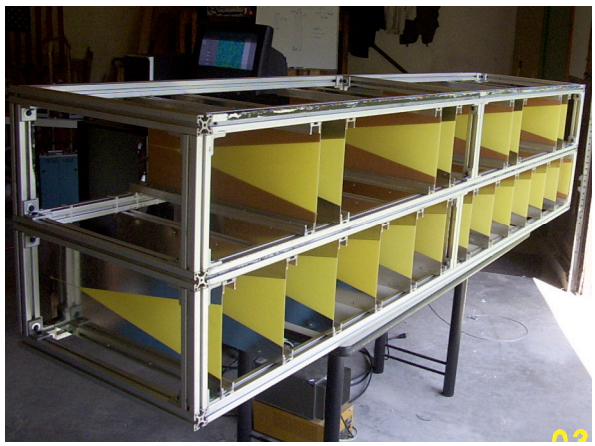

Figure 6 – The real-time S-band imaging radar antenna array.

A Labview GUI is programmed to control the fan-out solid state microwave switch matrices, pulse the transmitter, and digitize the de-chirped video signal. Real-time imaging is achieved by rapidly acquiring a range profile for each phase center across the array. As soon as a set of range profiles is acquired then calibration and background subtracted data are applied. Coherent integration is an optional software function but not used in the results shown in this paper. Calibration of the array is done for each of the 44 phase centers. After this is complete the data is processed using a SAR algorithm from [29] which was coded up in the Labview GUI. The resulting SAR image is displayed on the computer screen shown in Figure 5. This process is repeated over again until the user stops the program. With a 2.5 milli-second chirp rate this radar system is capable of displaying one SAR image every 1.9 seconds (approximately).

4. 0 Results

Imaging results of target scenes with various sizes of vertical rods and nails are shown in Figures 7 through 10. In these measurements the radar was chirping from approximately 2-4 GHz and was not using coherent integration. Background subtraction and calibration were used in all measurements. All data was acquired outdoors in the author's backyard with the radar system located in the garage pointed out towards the target scene as shown in Figures 5 and 6.

Figure 7 shows the resulting image of a group of 6 inch tall, 3/8 inch diameter, metal rods in a block 'S' configuration. This group of targets was located between 17 and 22 feet down range from the array. All targets are clearly shown and image SNR is good for all rods.

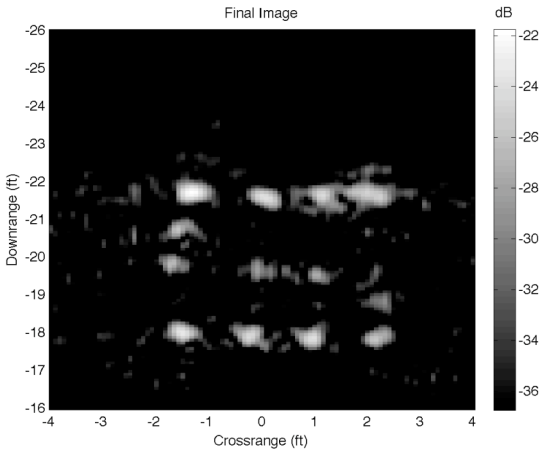

Figure 7 – Bolts.

Figure 8 shows a radar image of a group of 3 inch tall nails in the same block 'S' configuration at range of

approximately 14 to 19 feet away from the array. All targets are clearly shown except the return magnitude of the back row is lower than the front. Clutter is more apparent in this image.

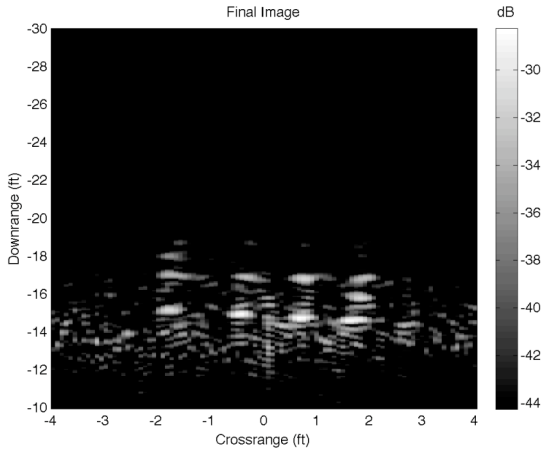

Figure 8 – 3 inch nails.

Figure 9 shows a radar image of a group of 2 inch tall nails in the block 'S' configuration at a range of approximately 14 to 19 feet away from the array. All targets are clearly shown with good signal to noise. The first row is noticeably brighter than the other rows. Some clutter is noticeable.

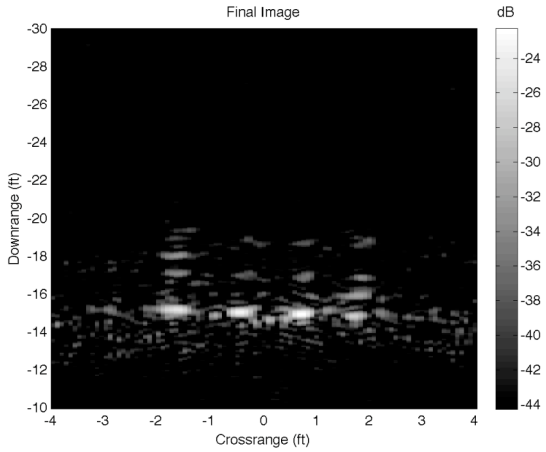

Figure 9 – 2 inch nails.

Figure 10 shows a radar image of a group of 1.25 inch tall nails the same block 'S' configuration as the others at a range of 14 to 19 feet from the array. All of the targets making up the block 'S' are clearly shown with good signal to noise ratio except for the top row.

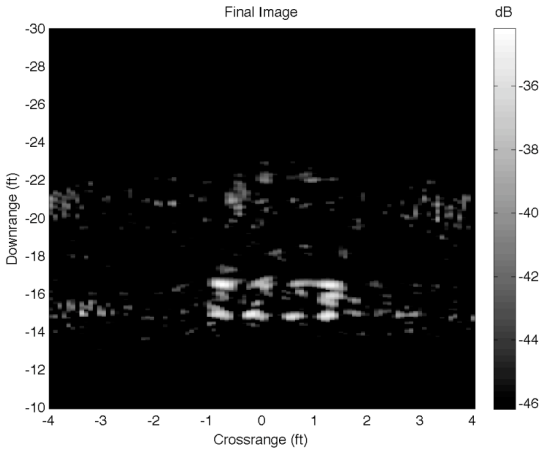

Figure 10 – 1.25 inch nails.

From these results it is shown that this S-band real time radar imaging system is capable of imaging groups of low RCS targets using low transmit power without the use of coherent integration.

5. 0 Summary

In this paper a highly sensitive, range gated, linear FM radar architecture was shown. This radar architecture was then used to build an S-band radar system. This radar system was integrated in to a switched aperture array. Software was written to SAR image target scenes at S-band in real-time with an image refresh rate of one image approximately every 1.9 seconds. The system was shown to be very sensitive; imaging target scenes of 1.25 inch tall nails using approximately 1 milli-watt of transmit power and no coherent integration. This radar system was originally developed for through-slab radar imaging but it was shown in this paper that RCS measurements are also possible. In addition to these applications this radar system could be useful in automotive radar, or any application requiring low power, high sensitivity, and range gating.

8.0 REFERENCES

[1] M. Mahfouz, A. Fathy, Y. Yang, E. E. Ali, A. Badawi, ``See-Through-Wall Imaging using Ultra Wideband Pulse Systems," IEEE Proceedings of the 34th Applied imagery and Pattern Recognition Workshop, 2005.

[2] Y. Yang, A. Fathy, ``Design and Implementation of a Low-Cost Real-Time Ultra-Wide Band See-Through-Wall Imaging Radar System," IEEE/MTT-S International Microwave Symposium, 3-8 June, 2007, pp.1476-1470.

[3] Y. Yang, C. Zhang, S. Lin, A. E. Fathy ``Developement of an Ultra Wideband Vivaldi Antenna Array," IEEE Antennas and Propagation Society

International Symposium, Vol. 1A, 2-8 July 2005, pp. 606-609.

[4] S. Nag, M. A. Barnes, T. Payment, G. W. Holladay, ``An Ultra-Wideband Through-Wall Radar for Detecting the Motion of People in Real Time,'' Radar Sensor Technology and Data Visualization, Proceedings of SPIE Volume 4744, 2002.

[5] M. A. Barnes, S. Nag, T. Payment, ``Covert Situational Awareness With Handheld Ultra-Wideband Short Pulse Radar,'' Radar Sensor Technology VI, Proceedings of SPIE Volume 4374, 2001.

[6] A. Berri, R. Daisy, ``High-Resolution Through-Wall Imaging,'' Sensors, and Command, Control, Communications, and Intelligence (C3I) Technologies for Homeland Security and Homeland Defense V, Proceedings of SPIE Volume 6201, 6201J, 2006.

[7] R. Benjamin, I. J. Craddock, E. McCutcheon, and R. Nilavalan, ``Through-Wall Imaging using Real-Aperture Radar,'' Sensors, and Command, Control, Communications, and Intelligence (C3I) Technologies for Homeland Security and Homeland Defense IV, Proceedings of SPIE Volume 5778, 20 May 2005, pp. 169-174.

[8] W. Zhiguo, L. Xi, F. Yuanchun, ``Moving Target Position with Through-Wall Radar,'' Proceedings of the CIE '06 International Conference on Radar, Oct. 2006.

[9] H. Burchett, ``Advances in Through Wall Radar for Search, Rescue and Security Applications,'' The Institution of Engineering and Technology Conference on Crime and Security, 13-14 June 2006, pp. 511-525.

[10] P. J. F. Swart, J. Schier, A. J. van Gemund, W. F. van der Zwan, J. P. Karelse, G. L. Reijns, P. van Genderen, L. P. Ligthart, H. T. Steenstra, ``The Colarado Multistatic FMCW Radar System,'' IEEE European Microwave Conference, October 1998, Vol. 2, pp. 449-454.

[11] V. Katkovnik, M. S. Lee, Y. H. Kim, ``High-Resolution Signal Processing for a Switch Antenna Array FMCW Radar with a Single Channel Receiver,'' IEEE Proceedings of Sensor Array and Multichannel Signal Processing, 4-6 August 2002, pp. 543-547.

[12] M. S. Lee, V. Katkovnik, Y. H. Kim, ``System Modeling and Signal Processing for a Switch Antenna Array,'' IEEE Transactions on Signal Processing, Vol. 52, Issue 6, June 2004, pp. 1513-1523.

[13] G. L. Charvat, L. C. Kempel, C. Coleman, “A Low-Power High-Sensitivity X-Band Rail SAR Imaging System,” IEEE Antennas and Propagation Magazine, Vol. 50, No 3, June 2008, pp. 108-115.

[14] G. L. Charvat, ``A Low-Power Radar Imaging System,'' Ph.D. dissertation, Dept. of Electrical and Computer Engineering, Michigan State University, East Lansing, MI, 2007.

[15] G.L. Charvat, ``Low-Cost, High Resolution X-Band Laboratory Radar System for Synthetic Aperture Radar Applications,'' Antenna Measurement Techniques Association Conference, Austin, Texas, October 2006.

[16] M. P. G. Capelli, ``Radio Altimeter,'' IRE Transactions on Aeronautical and Navigational Electronics, Vol. 1, June 1954, pp. 3-7.

[17] F. T. Wimberly, J. F. Lane, ``The AN/APN-22 Radio Altimeter,'' IRE Transactions on Aeronautical and Navigational Engineering, Vol. 1, June 1954, pp. 8-14.

[18] A. Black, K. E. Buecks, A. H. Heaton, ``Improved Radio Altimeter,'' Wireless World, Vol. 60, March 1954, pp. 138-140.

[19] A. G. Stove, ``Linear FMCW radar techniques,'' IEE Proceedings of Radar and Signal Processing, Vol. 139, October 1992, pp. 343-350.

[20] *The ARRL Handbook, 71st Edition*, The American Radio Relay League, Inc., Newington, CT, 1994.

[21] U. L. Rhode, J. Whitaker, T. T. N. Bucher, *Communications Receivers, 2nd Ed.*, McGraw-Hill, New York, NY, 1996.

[22] R. Janaswamy, D. H. Schaubert, and D. M. Pozar, ``Analysis of the transverse electromagnetic mode linearly tapered slot antenna,'' Radio Science, Volume 21, No. 5, pp. 797-804, September-October 1986.

[23] R. Janaswamy, D. H. Schaubert, ``Analysis of the Tapered Slot Antenna,'' IEEE Transactions on Antennas and Propagation, Vol. AP-35, No. 9, September 1987, pp. 1058-1065.

[24] R. Janaswamy, ``An Accurate Moment Method Model for the Tapered Slot Antenna,'' IEEE Transactions on Antennas and Propagation, Vol. 37, No. 12, December 1989.

[25] Y. S. Kim, S. Yngvesson, ``Characterization of Tapered Slot Antenna Feeds and Arrays,'' IEEE Transactions on Antennas and Propagation, Vol. 38, No. 10, October 1990.

[26] P. S. Kooi, T. S. Yeo, M. S. Leong, ``Parametric Studies of the Linearly Tapered Slot Antenna (LTSA),'' IEEE Microwave and Optical Technology Letters, Vol. 4, No. 5, April 1991.

[27] E. Thiele, A. Taflove, ``FD-TD Analysis of Vivaldi Flared Horn Antennas and Arrays,'' IEEE Transactions on Antennas and Propagation, Vol. 42, No. 5, May 1994.

[28] X. D. Wu, and K. Chang, ``Compact Wideband Integrated Active Slot Antenna Amplifier," IEEE Electronics Letters, Vol. 29, No. 5, 4 March 1993.

[29] W.G. Carrara, R.S. Goodman, and R.M. Majewski, *Spotlight Synthetic Aperture Radar Signal Processing Algorithms*, Artech House, Boston, MA, 1995.